ARCHIVES OF ELECTRICAL ENGINEERING VOL. 61(2), pp. 267-276 (2012)

DOI 10.2478/v10171-012-0022-2

Determination of best rotor length in solid-rotor induction motor with axial slitting

MARIUSZ JAGIELA, TOMASZ GARBIEC

Department of Electrical, Automatic Control and Computer Engineering
Opole University of Technology,
45-758 Opole, ul. Proszkowska 76,

e-mail m.jagiela@po.opole.pl, t.grabiec@doktorant.po.edu.pl

(Received: 03.02.2012, revised: 10.03.2012)

Abstract: The efficiency of the solid-rotor induction machines depends on axial length of rotor (including the end-regions). Determination of the best axial length is problematic because of current density distribution in the end-regions and also because of absence of dedicated methods and models. This work proposes a method that circumvents this difficulty. It is based on the numerical determination of a dimensionless rotor-end factor using a combination of three- and two-dimensional finite element models restricted to the motor rotor. Such the end factor can be used in both analytical and numerical model of the machine in order to determine the typical performance characteristics. In this work, using this method, we determined an optimal length of the slitted solid rotor of a motor operating at 12 000 rpm, that maximizes the motor efficiency. The results of computations and measurements, carried out on the laboratory test-stand, are presented.

Key words: solid-rotor, induction motor, end effects, rotor-end factor, eddy currents

1. Introduction

The majority of industrial applications of high-speed electrical machines are related with tendency to reduce an intake and waste of electrical energy wherever it is possible. The overall energy demand of some industrial drives, like drives of certain pumps and gas compressors, could be rationalized by means of increasing the operating speed. This is because the efficiencies of certain flow machines rise with the speed of operation [1-5].

There are many solutions of magnetic circuits for the high-speed machines [1]. Almost all types of electric machines are utilized in the high-speed versions. Among them is a mild-steel, solid-rotor induction machine that, due to rigid structure and integrity, can be operated with the highest currently required rotational speeds. One additional useful property of this machine is its ability to operate in harsh environments like exhaust and natural gases. A disadvantage of such the structure is relatively poor performance compared with the squirrel-cage or

permanent-magnet machines. Also, designing these machines significantly differs from that of the squirrel-cage ones due to large impact of rotor-end regions and stray losses [3, 5]. It is known that the overall losses in the solid rotor can be reduced and the machine power factor can be significantly gained by means of application of axial slitting, as shown in Fig. 1.

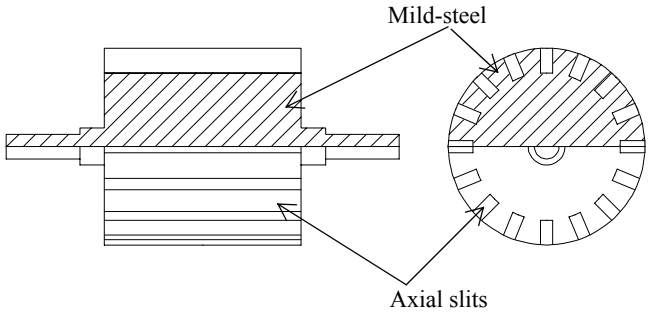

Fig. 1. Axially slitted solid rotor having slits throughout the whole length

Slitting reduces the equivalent surface impedance of the rotor by increasing the penetration depth by the magnetic field in radial direction.

In designing these motors, the majority of methods (including analytical and numerical approaches) take account of only one (normal) component of the rotor current density. The two remaining (tangential) components are accounted for using simplifications. These simplifications regard application of the dimensionless correction factors for the rotor conductivity so as to bring the rotor power closer to that in real system. This technique is known under common name "effective conductivity approach". An unquestionable advantage of such an approach is its applicability in both numerical and analytical methods [3-10].

There are a few different analytic expressions for the rotor-end factors available [6-10]. Although for the smooth rotors (unslitted), these generally provide proper estimates of the impact of rotor-end effect, neither can be applied to the slitted rotors due to more complicated distribution of current density which additionally varies with frequency. Consequently, it should be expected that the rotor-end factor of such the motor also depends on frequency (slip). In this connection, the task related with designing the length of the slitted rotor cannot be reliably solved without recalling the three-dimensional eddy-current analysis. However, it is well known that application of such the models in case of induction motors relates with conducting extensive computer simulations that make the process of designing especially laborious.

This work proposes to estimate the slitted rotor end factor numerically. This factor is determined as function of frequency and can be used in both analytical and numerical method of designing that deals with only one component of the vector of current density. The results obtained within the proposed approach are unique and are valuable from the designer point of view. This is confirmed by measurements carried out on the laboratory machine.

2. Laboratory motor and test-stand

The laboratory test-stand for the considered motor is shown depicted in Fig. 2. Table 1 summarizes the technical specifications. The motor is driven from a three-phase quasi-square inverter. Forced fluid cooling is used.

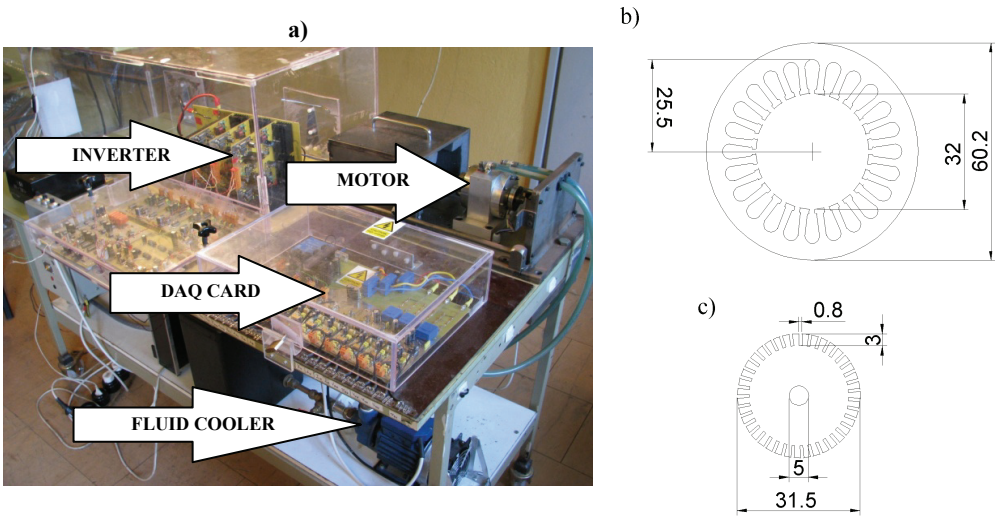

Fig. 2. Laboratory test-stand a), stator b) and rotor c) of the considered motor with dimensions

Table 1. Technical specifications of the solid-rotor induction motor with slitted rotor

Nominal power	330 W
Nominal voltage (star connection)	150 V
Frequency	500 Hz
Rated slip	0.2
Number of pole-pairs	2
Number of stator slots	24
Stator length Stator bore diameter Air-gap length Rotor length	32 mm 32 mm 0.5 mm 40 mm
Winding type	two-layer, fully-pitched
Number of turns per slot	18
Number of rotor slits	40

3. Determination of rotor-end factor for slitted rotor

One fundamental assumption within the approach used here, is that an overall effect due to rotor end region can be uniquely characterized by ratio of powers calculated in the three-

dimensional (accounting for end effect) and two-dimensional (neglecting end effect) system. This assumption has some support in the way how the rotor-end factor is generally incorporated into "non-three-dimensional models", which refers to all simplified approaches not directly accounting for the tangential components of current density vector in the rotor. As it was mentioned in the introductory section, the rotor-end factor is introduced in such a way as to bring the rotor power calculated in the two-dimensional system closer to that in real rotor. Both powers are dependent on frequency of excitation f_s, thus at a given frequency:

$$P_{3d}(f_s) = P_{2d}(f_s)k_e(f_s), \tag{1}$$

consequently:

$$k_e(f_s) = \frac{P_{3d}(f_s)}{P_{2d}(f_s)}, \tag{2}$$

where $P_{3d}(f_s)$ and $P_{2d}(f_s)$ are calculated separately using two different models in the same conditions regarding frequency and magnitude of excitation. Four important notes should be added here.

- Evaluation of (2) does not require considering an entire machine, but only the region restricted to the rotor. This can be realized by imposing appropriate boundary condition modeling distribution of an air-gap flux density.
- The rotor-end factor (2) is attributed only to the fundamental harmonic of an air-gap flux density, similarly as in more traditional approaches.
- The model for computation of power $P_{3d}(f_s)$ cannot be nonlinear as otherwise it would be computationally too expensive to be applicable in a process of designing based on trial-and-error search. Consequently, a special care must be taken with respect to the rotor permeability used.
- Owing to the above, the rotor-end factor calculated in this way is independent of excitation (magnitude of an air-gap flux density) used at the boundary.

In order to determine power $P_{3d}(f_s)$ a three-dimensional finite element model is elaborated. The model is based on the formulation for modified complex magnetic vector potential incorporated in such a way as at the given pulsation ω:

$$\underline{\mathbf{A}} = \underline{\mathbf{A}}' + (\mathrm{j}\omega)^{-1}\mathbf{grad}\underline{V}, \tag{3}$$

where $\underline{\mathbf{A}}$ is complex magnetic vector potential, j is the imaginary unit and $\underline{V}$ is complex electric scalar potential. The equation governing the electromagnetic field has form:

$$\mathbf{curl}\frac{1}{\mu}\mathbf{curl}\mathbf{A}' = -\mathrm{j}\omega\sigma\mathbf{A}', \tag{4}$$

where μ is the magnetic permeability. Using a discrete geometric approach and a cylindrical curvilinear hexahedral element, equation (4) in a discrete space, is represented by [12-15]:

$$\mathbf{C}^T\mathbf{v}\mathbf{C}\underline{\mathbf{a}} = -\mathrm{j}\omega\boldsymbol{\sigma}\underline{\mathbf{a}}, \tag{5}$$

where: $\underline{\mathbf{a}}$ – vector of circulations of $\mathbf{A}'$ along element edges, $\mathbf{C}$ – matrix of incidences of element edges with element faces, $\boldsymbol{\nu}$ is a constitutive positive definite matrix of magnetic reluctivity, $\boldsymbol{\sigma}$ is a constitutive positive definite matrix of electric conductivity. A more detailed presentation on how these matrices are constructed can be found in [12-15]. Power $P_{3d}(f_s)$ is calculated after solution of (5) using nonhomogeneous boundary condition of first kind, which refers to the mentioned distribution of the fundamental harmonic of radial component of magnetic flux density in the motor air-gap. This boundary condition is imposed on the component of $\mathbf{A}'$ in direction parallel to the motor shaft, whilst the two remaining components are set to zero at this boundary (see Fig. 3).

Determination of power $P_{2d}(f_s)$ requires creation of a separate two-dimensional model having exactly the same dimensions as the three-dimensional model and the same boundary condition imposed. In practice creation of such the model is very straightforward because in the system of equations (5) it requires taking account of circulations of $\mathbf{A}'$ only in axial direction and neglecting equations for the two remaining directions.

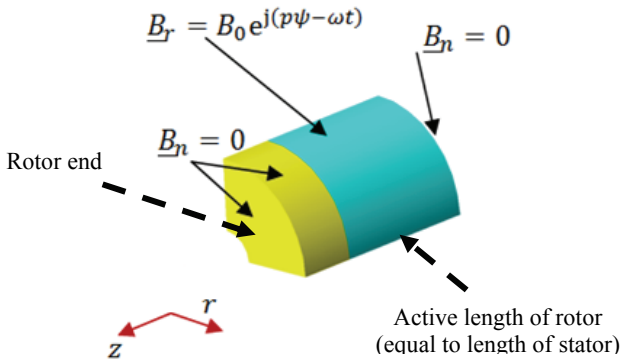

Fig. 3. Selection of region of analysis for three-dimensional computations of current density: r, ψ, z are spatial coordinates, $\underline{B}_n$ denotes component of magnetic flux density normal to boundary, p denotes the number of motor pole-pairs, B_0 is the magnitude of radial component of magnetic flux density. Only one pole is considered using periodicity conditions

As it was mentioned, the method is based on assumption of constant rotor permeability. In real machine it is evident that variation of rotor slip relates with variation of an air-gap flux density. Consequently, selection of the most appropriate value of rotor permeability it is not an easy task. A plenty of numerical experiments carried out by the authors show that the best is to use an average value of relative permeability that corresponds with nominal point of operation of the motor. Here, this value equals 160.

Figure 4 depicts distributions of current density at 20 per cent slip corresponding with two different rotor lengths. Main value of the vector plots involves the visibility of complexity of the distributions. Based on that it can be guessed why the available analytic estimates of the rotor-end effect used to this date cannot properly represent the slitted rotor.

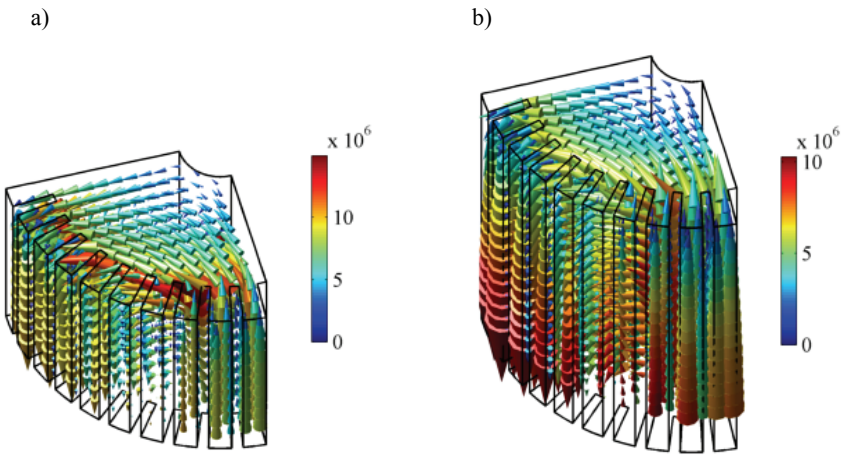

Fig. 4. Distribution of current density in the rotor (A/m^2) at 20 per cent slip in the rotor having the same length as stator a), in the rotor being 75 per cent longer than stator b)

Looking in Figure 4 it can be noticed that the distribution of current density is highly nonuniform in each direction. In region of slits the current path tends to leave the teeth prior to entering the end region. This behavior of current density cannot be properly reflected in the two-dimensional model because some portions of power density, are not present on the two-dimensional plane of analysis. This problem can be circumvented if two rotor-end factors are distinguished, namely one for the region of teeth and one for the region of the uniform cylinder. This is done in Figure 5.

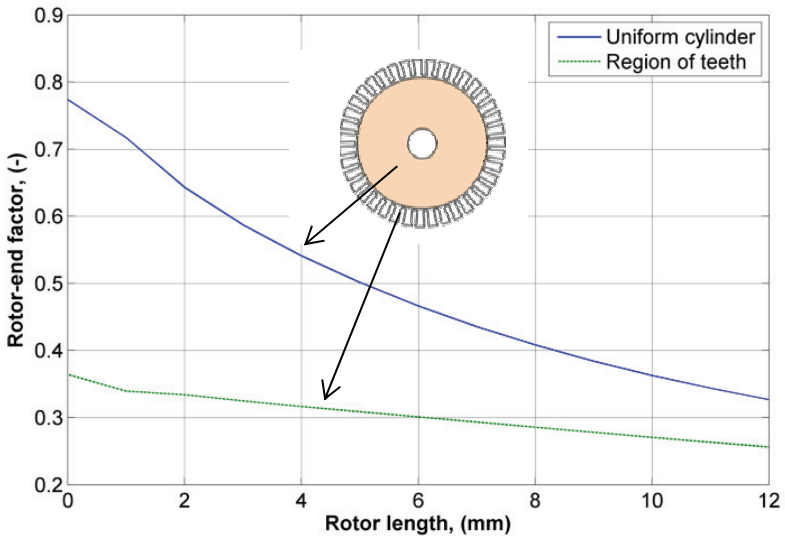

Fig. 5. Variation of rotor-end factors with length of rotor-end region at 20 per cent slip, determined from equation (2). Calculations carried out at nominal conditions of operation

4. Determination of the best rotor length

Looking in Figure 5 it can be deduced that extension of the rotor length increases the effective impedance (effective conductivity drops down). It is thus expected that the best, from the point of view of electromechanical quantities, is the shortest rotor. In such the case, owing to the constant outer diameter, the rotor has the smallest moment of inertia. In order to provide quantitative information, an analysis will be performed using a nonlinear, circuit-driven, two-dimensional frequency-domain finite element model accounting for stator core loss and also, in a simplified way, for rotor loss due to higher harmonics. It is well known that models of this type are not very precise if strong saturation effects and losses due to higher harmonics must be accounted for. Here, it can be said that this model is sufficiently accurate owing to requirements of this design. A link between analysis that has led to determination of rotor-end factors (see Fig. 5) and this model, relies upon introducing the effective rotor conductivity $\hat{\sigma}(f_s)$ in such way as

$$\hat{\sigma}(f_s) = \sigma k_e(f_s). \tag{6}$$

This conductivity replaces the physical conductivity of respectively, the region of teeth and the region of central cylinder of the rotor in the considered two-dimensional finite element model. Figure 6 depicts flux distribution over motor cross-section corresponding to 20 per cent slip. Validation of the model against measurements of torque, power factor and rms phase current for a 40 mm long rotor (length of end region equal to 4 mm), that was designed based on empirical guess, is shown plotted in Fig. 7.

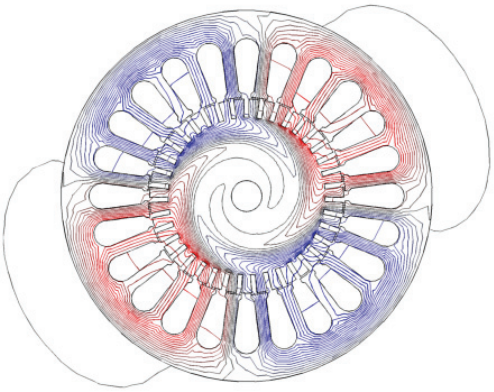

Fig. 6. Flux density distribution at rated conditions of operation

As it can be seen, the model provides assessment of motor quantities within 13 per cent of discrepancy for the considered rotor length, and this confirms its validity. Figures 8a-c depict variations of motor quantities with length of the rotor-end region at nominal conditions of operation. It is clear that the best from the efficiency point of view is the shortest possible

rotor with no rotor overhang beyond the stator. This result is not surprising because the shorter rotor is the smaller equivalent rotor impedance it corresonds.

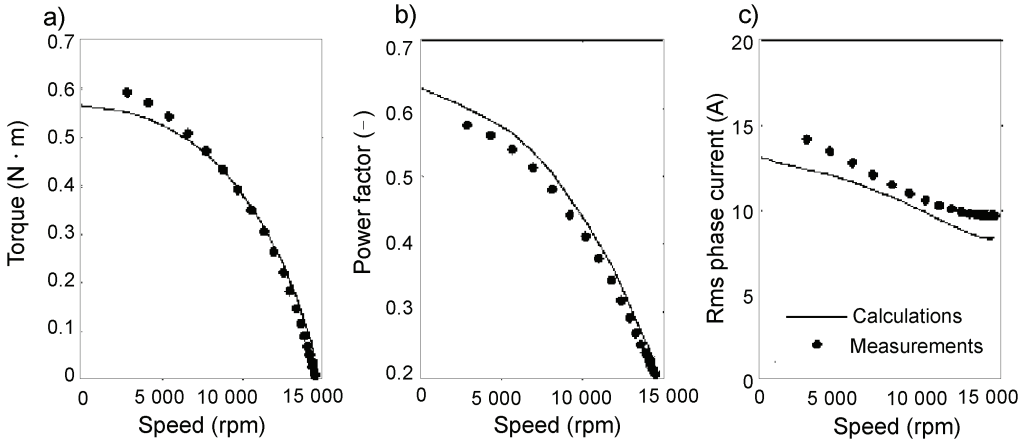

Fig. 7. Computed and measured variations of torque a), power factor b) and rms phase current c) vs. rotor speed at nominal frequency and voltage

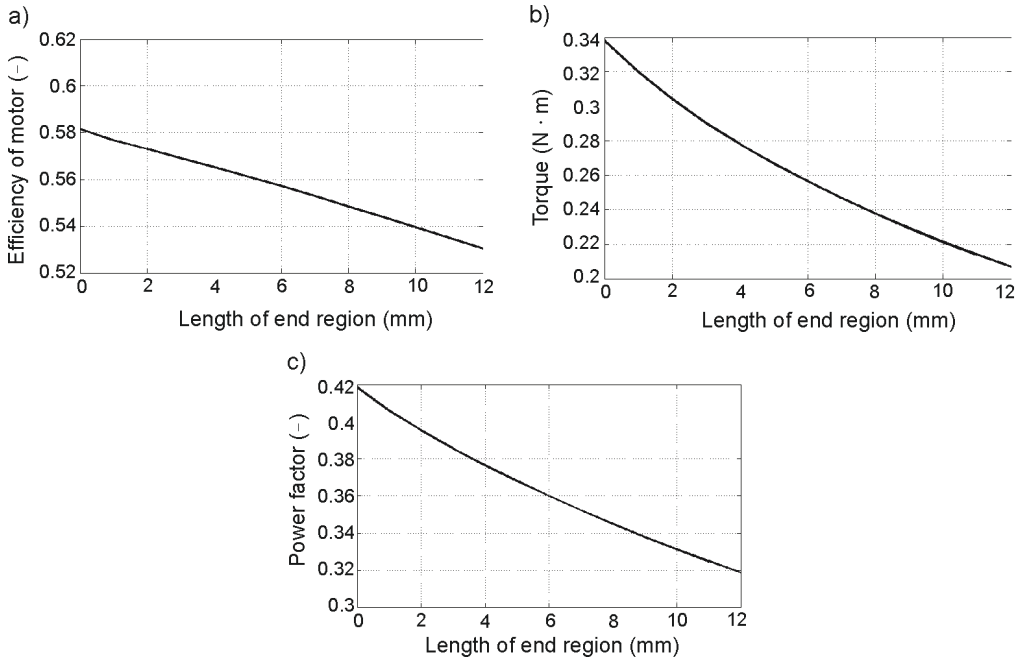

Fig. 8. Variation of motor efficiency a), torque b) and power factor c) with length of the rotor-end region. Calculations carried out at nominal conditions of operation

5. Conclusion

This work demonstrated how to deal with the problem of determination of the best length of the slitted solid rotor of an induction motor. The presented method of numerical determination of the rotor-end can be applied with respect to motors having arbitrary rotor dimensions and number of poles. It can be considered as a computationally-efficient improvement of the approaches based on effective conductivity that are used to this date. Determination of variations plotted in Fig. 5 takes only 30 minutes on the contemporary desktop computer, which is only a fraction of time required for solution of a complete three-dimensional problem using a comprehensive model.

It should be mentioned that there are many options regarding construction of the rotor end region. In this work we analyzed the rotor having slits throughout whole length although references also reports on the slitted rotors with the end rings attached to the end regions. These end-rings can be made of either the same or different material than the rotor. The approach based on distinction of two different end factors for the two different rotor regions presented in this work is applicable directly to such rotor structures.

Acknowledgment

This work is supported by project No. NN 510 700840 from Polish Ministry of Science and Higher Education. This work is supported by European Social Fund.

References

[1] Rahman M.A., Chiba A., Fukao T., *Super high speed electrical machines – summary.* Proc. of Power Engineering Society General Meeting, Denver, USA, 10 June, 2004, 2: 1272-1275 (2004).

[2] Aho T., Sihvo V., Nerg J., Pyrhönen J., *Rotor materials for medium-speed solid-rotor induction motors.* Proc. of IEEE International Conference on Electric Machines and Drives (IEMDC 2007), Antalya, Turkey, 3-5 May, 2007, pp. 525-530 (2007).

[3] Huppunen J., *High-speed solid-rotor induction machine – electromagnetic calculation and design.* Ph. D. Diss., Acta Universitatis Lappeenrantaensis, Lappeenranta (2004).

[4] Zhou H., Wang F., *Comparative study on high speed induction machine with different rotor structures.* Proceedings of International Conference on Electrical Machines and Systems, Seoul, South Korea, 8-11 October, 2007, pp. 1009-1012.

[5] Bumby J. R., Spooner E., Jagiela M., Equivalent circuit analysis of solid-rotor induction machines with reference to turbocharger accelerator applications, IEE Proceedings, Electric Power Applications 153(1): pp. 31-39 (2006).

[6] Trickey P.H., *Induction motor resistance ring width.* Transactions of American Institute of Electrical Engineers, February, 1936, 55(2): 144-150 (1936).

[7] Russell R.L., Norsworthy K.H., *Eddy currents and wall losses in screened-rotor induction motors.* Proc. of IEE, Part A: Power Engineering, April 1958, 105(20): 163-175.

[8] Yee H., Effects of finite length in solid-rotor induction machines, IEE Proc., August 1971, 118(8): 1025-1033.

[9] O'Kelly D., *Theory and performance of solid-rotor induction and hysteresis machines.* IEE Proc., May 1976, 123(5): 421-428.

[10] Woolley I., Chalmers B. J., *End effects in unlaminated-rotor induction machines.* IEE Proc., June 1973, 120(6): 641-646.

[11] Jagiela M., Garbiec T., *Evaluation of rotor-end factors in the solid rotor induction motors.* IEEE Transactions on Magnetics, January, 2012, 48(1), (2012).
[12] Codecasa L., Dular P., Specogna R., Trevisan F., *Time-domain Geometric Eddy-Current A Formulation for Hexahedral Grids.* IEEE Transactions on Magnetics 46(8): 3301-3304 (2010).
[13] Demenko A., *Obwodowe modele układów z polem elektromagnetycznym* (*Circuit models of systems with electromagnetic field.* In Polish), Poznan University of Technology Academic Press, Poznan (2004).
[14] Demenko A., Wojciechowski R., Sykulski J., *On the Equivalence of Finite Element and Finite Integration Formulations.* IEEE Transactions on Magnetics 46(8): 3169-3172 (2010).
[15] Jagiela M., Garbiec T., *Three-dimensional calculations of eddy-current distribution – application of description of the finite element geometrical forms.* (In Polish), Electrical Review 2, Sigma-Not, pp. 1-4 (2011).